

Lightcurve Classification in Massive Variability Surveys I: Microlensing

Vasily Belokurov¹, N. Wyn Evans^{1,2}, Yann Le Du¹

¹ *Theoretical Physics, Department of Physics, 1 Keble Road, Oxford, OX1 3NP, UK*

² *Institute of Astronomy, Madingley Rd, Cambridge, CB3 0HA, UK*

19 March 2018

ABSTRACT

This paper exploits neural networks to provide a fast and automatic way to classify lightcurves in massive photometric datasets. As an example, we provide a working neural network that can distinguish microlensing lightcurves from other forms of variability, such as eruptive, pulsating, cataclysmic and eclipsing variable stars. The network has five input neurons, a hidden layer of five neurons and one output neuron. The five input variables for the network are extracted by spectral analysis from the lightcurve datapoints and are optimised for the identification of a single, symmetric, microlensing bump. The output of the network is the posterior probability of microlensing.

The committee of neural networks successfully passes tests on noisy data taken by the MACHO collaboration. When used to process ~ 5000 lightcurves on a typical tile towards the bulge, the network cleanly identifies the single microlensing event. When fed with a sub-sample of 36 lightcurves identified by the MACHO collaboration as microlensing, the network corroborates this verdict in the case of 27 events, but classifies the remaining 9 events as other forms of variability. For some of these discrepant events, it looks as though there are secondary bumps or the bump is noisy or not properly contained. Neural networks naturally allow for the possibility of novelty detection – that is, new or unexpected phenomena which we may want to follow up. The advantages of neural networks for microlensing rate calculations, as well as the future developments of massive variability surveys, are both briefly discussed.

Key words: gravitational lensing – variable stars – data processing

1 INTRODUCTION

Variability in the sky has been known for thousands of years, but our understanding of variable sources remains very incomplete. Some of the most interesting objects in the sky are transient. These include supernovae, microlensed stars, near-Earth or killer asteroids (which are transient because of their exceptionally large proper motions) optical flashes associated with gamma-ray bursts and stars undergoing short-lived but key stages of stellar evolution like the helium core flash and so on. All these objects are rare. To hunt them down in a systematic way means that we must record images, process the data in real-time (or nearly so), recognise the events from their lightcurves and archive them.

The earliest examples of massive transient astronomy searches are the microlensing surveys like MACHO ¹, EROS ² and OGLE ³. Typically, the surveys monitored

$\sim 5 \times 10^6$ stars a few times every night over several years in the directions of the Galactic Bulge and the Magellanic Clouds, yielding $\sim 10^{10}$ photometric measurements. Out of the $\sim 10^5$ sources which were variable, the surveys tried to identify $\sim 10^2$ true microlensing events. The selection criteria typically involved the imposition of sets of cuts to ensure good lightcurve coverage and a steady baseline flux, to require a single bump and thus eliminate common forms of stellar variability and to require a good statistical fit to the achromatic standard microlensing lightcurve and so on. Many of the cuts developed through trial and error, and evolved as the experiments progressed (e.g., Alcock et al. 1997, 2000a). Unambiguous identification of microlensing events was sometimes not possible, and the collaborations sometimes reported their results in terms of two sets, one of high quality events (any lightcurve that was undoubtedly microlensing) and one of possible events (any lightcurve with a unique peak and a flat baseline). Sometimes the cuts even eliminated interesting events – for example, the longest ever microlensing event OGLE-1999-BUL-32 was originally

¹ <http://www.macho.anu.edu.au/>

² <http://eros.in2p3.fr/>

³ <http://sirius.astrouw.edu.pl/~ogle/>

missed as its baseline flux was not constant and so failed one of the imposed cuts (Mao et al. 2002).

Additionally, microlensing alert or early warning systems (e.g., Udalski et al. 1994) work by reducing the number of candidates to manageable amounts. Each night's candidates are individually examined for the onset of microlensing. Even for surveys as large as OGLE II, this worked well. However, still larger surveys are planned for the future and therefore it becomes important to automate the procedure and issue alerts without human intervention.

The microlensing experiments are of course not the only massive photometry searches being conducted by astronomers at the moment. There are also collaborations primarily looking for supernovae (e.g., The Supernovae Cosmology Project), optical flashes related to gamma-ray bursts (ROTSE) and near-Earth asteroids (NEAT and LINEAR). More generally, as Paczyński (2001, 2002) has emphasised, the monitoring of the optical sky for variability is likely to enjoy a huge resurgence over the coming decade given the low cost of robotic telescopes. The very near future will see terabyte datasets of lightcurves routinely available to astronomers. Such datasets will contain complete samples of variable stars of all types, as well as the very rare objects or events which primarily motivate the search. It is a urgent and important problem to automate the classification of lightcurves in massive variability surveys.

This paper argues that new analysis methods based on neural networks will enable us to pinpoint and identify scarce transient objects in such huge datasets. Our illustrative example is the identification of scarce microlensing events against the background of variable stars. However, we envisage that the applicability of the technique is much wider.

2 MICROLENSING LIGHTCURVES

At any instant, the probability that a source star in the Galaxy shows the microlensing effect is $\lesssim 10^{-6}$. Microlensing events are hugely outnumbered by stellar variability which is at least a hundred thousand times more common. The lightcurve classification problem is to devise algorithms that diagnose the different kinds of variability. For applications to microlensing, the algorithm must distinguish microlensing from other sources of variability (whether intrinsic or extrinsic).

Let us assume a single, point-like, dark lens. The microlensing lightcurve has a characteristic form written down by Paczyński (1986). The lightcurve is symmetric and achromatic. As the probability of microlensing is so low, the variability must not repeat. Microlensing is readily distinguished from some, but unfortunately not all, forms of stellar variability. A cautionary history is provide by the fate of the candidate event EROS-LMC-2. This was one of the microlensing candidates uncovered by the photographic plate search of the first phase of the EROS experiment towards the Large Magellanic Cloud (Ansari et al. 1996). Although the source star of EROS-LMC-2 was known to be variable at a low level (Ansari et al. 1995), nonetheless microlensing seemed favoured by the excellent fit of the lightcurve to the data-points. However, there was a substantial second bump in the lightcurve eight years after the first, and EROS-LMC-2 was

then discarded as a microlensing candidate (Lasserre et al. 2000).

The background in microlensing databases is composed of periodic variables (e.g., Cepheids, RR Lyrae), eruptive variables (e.g., dwarf novae, classical novae), semi-regular variables (e.g., bumpers) and the supernovae occurring in galaxies behind the source population. Of these, the most troublesome in microlensing surveys towards the Magellanic Clouds and Andromeda are the bumpers and the novae-like objects. Although SNe Ia have reasonably well-understood lightcurves, the same is not true of other types of supernovae which can mimic microlensing rather well (for example, events 22 and 26 of Alcock et al. 2000a). Long period bumpers may be present as single bumps even in 5 seasons worth of data and they can be well-fit by the standard microlensing lightcurve.

Let us stress that the identification of microlensing events remains an awkward – and not fully solved – problem. For example, it probably lies at the heart of the seeming discord between the results of the MACHO and EROS experiments towards the Large Magellanic Cloud (LMC). The MACHO group identified between 13 and 17 events towards the LMC, whereas the competing EROS group found only 3 (Alcock et al. 2000a, Lasserre et al. 2000). Although the exposure times and field locations between the two experiments do vary, nonetheless the rate found by MACHO is at least twice than that found by EROS. This same disparity is also seen in the experiments towards the Galactic Bulge, as MACHO find an optical depth to microlensing of $\sim 3.23 \times 10^{-6}$ (Alcock et al. 2000b), whereas the EROS value is about half of this (Afonso et al 2003). Possible explanations are that the MACHO selection algorithm may be too loose (causing contamination with other variable sources), or that the EROS selection algorithm may be too harsh (causing genuine events to be discarded). It is here that neural networks may be able to make a decisive contribution.

3 AN INFORMAL INTRODUCTION TO NEURAL NETWORKS

Neural networks have been used before for pattern recognition tasks in physics (e.g., Bishop 1995). In particular, they are often used in high energy physics experiments as triggers to select interesting events from large datasets (Müller, Reinhardt & Strickland 1995, chapter 8). Recent astronomical applications include classification of optical stellar spectra (Bailer-Jones et al. 1997) and galaxy type (Lahav et al. 1995), object detection in wide field imaging (Andreon et al. 2000) and predictions of astronomical time series (e.g., Conway 1998, Perdang & Serre 1998). There has also been a recent report of preliminary results on automatic lightcurve classification by the ROTSE collaboration (Wozniak et al. 2001). An interesting review of a number of astronomical applications is in Storrie-Lombardi & Lahav (1994).

In a neural network, the neurons are arranged in layers. The input data is fed to the bottommost layer. The output value emerges from the topmost layer, the intervening layers are hidden. The values of the neurons in any layer a_j are calculated via

$$a_j = \sum_i w_{ji} z_i. \quad (1)$$

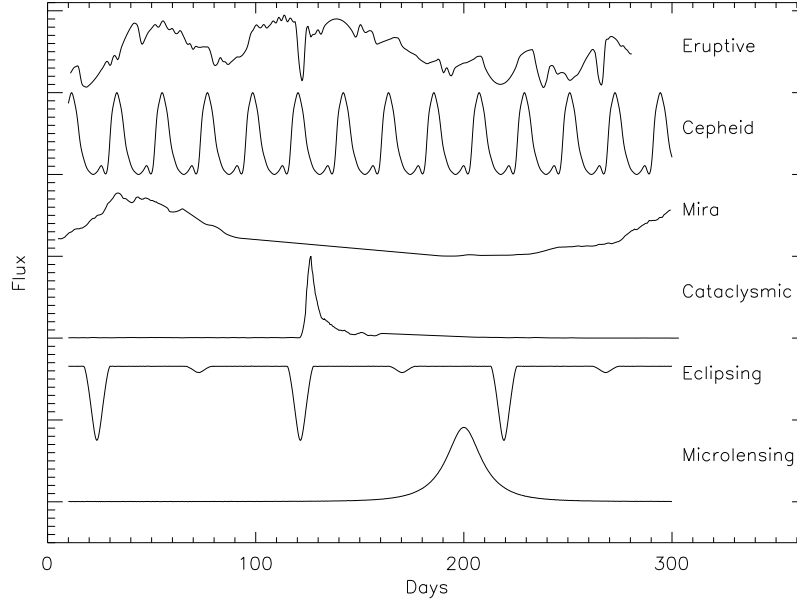


Figure 1. This shows sample lightcurves of different types of variability included in the training and validation sets.

Variable	Reference
Eruptive	van Genderen (1995), AAVSO
Pulsating	Antonello & Morelli (1996), AAVSO
Cataclysmic	Hamuy et al. (1996), AAVSO
Eclipsing	Brancewicz, Dworak (1980)

Table 1. Sources of lightcurves of variable stars. AAVSO is the American Association of Variable Star Observers.

Here, w_{ji} are the synaptic weights of the j th neuron with respect to the i th neuron and z_i are the activation values. The activation value is computed from the value on the neuron via an activation function g

$$z_i = g(a_i). \quad (2)$$

As an activation function, we use the logistic function

$$g(a) = \frac{1}{1 + \exp(-a)}, \quad (3)$$

which allows us to interpret the outputs of the network as *a posteriori* probabilities (Bishop 1995, chapters 3,6).

We start with a sequence of input units (the “patterns”) for which the desired values of the output (the “targets”) are known. This is called the training set. Given the patterns and a set of weights, we can construct an error function E which quantifies the performance of the network. We want to obtain the weights w_{ji} that minimise the error function over the training set using a steepest descent scheme.

We begin with random values for the weights and perform a sequence of iterative up-dates using a variant of back-propagation as the learning algorithm. The error derivatives with respect to the weights are

$$\frac{\partial E^n}{\partial w_{ji}} = \delta_j^n z_i^n, \quad \delta_j \equiv \frac{\partial E^n}{\partial a_j}, \quad (4)$$

where n labels the pattern. Using the chain rule, we obtain the back-propagation formula

$$\delta_j^n = g'(a_j) \sum_k w_{kj} \delta_k^n, \quad (5)$$

which shows how the values of δ_j^n propagate through the network, given the target value. In each iteration, the weights are up-dated according to the following rule

$$\Delta w_{ij} = -\eta \sum_n \delta_j^n z_i^n, \quad (6)$$

where η is the constant learning rate. The sum is performed over all the patterns. This is equivalent to the steepest descent method of minimizing the error. In practice, we use a refinement of this algorithm, called resilient back-propagation, which helps to prevent entrapment in local minima (see e.g., Bishop 1995, section 7.5.3).

As the network is converging to a minimum, it is important to prevent overtraining. This is done by feeding a different set of patterns (the “validation set”) to the network. The errors over the patterns in the training and the validation sets are separately computed. The training process is stopped just before the error in the validation set begins to rise. Finally, the performance of the fully trained network can be assessed with a third set of patterns (the “test set”).

It is important to ensure that the training, validation and test sets do not contain any identical patterns.

4 IMPLEMENTATION

The experiments described below use the Stuttgart Neural Network Simulator (“<http://www-ra.informatik.uni-tuebingen.de/SNNS>”). Our network is composed of one input layer, one hidden layer and one output layer. The hidden layer is fully connected to the input and output layers. There are 5 neurons in the input layer, 5 neurons in the hidden layer and one neuron in the output layer. The value of the output neuron gives the probability that the event is microlensing. The reason for the choice of 5 input neurons will become obvious shortly.

4.1 The Training and the Validation Sets

There are three types of lightcurves in the training set – simulated microlensing events, variable star lightcurves from archival sources, and sample lightcurves from a microlensing experiment (in this case, the MACHO experiment).

Simulated microlensing events are generated by randomly choosing an impact parameter, an Einstein crossing time between 7 days and 365 days and a time when the event reaches maximum. Random gaussian noise is added with a dispersion in the range from 0.1 to 20 % of the maximum flux. The lightcurves are sparsely sampled using the MACHO sampling.

Variable stars may be divided into periodic variables and eruptive/cataclysmic variables. The former are usually easier to distinguish from microlensing than the latter, always provided more than one period can be detected in the sampled datastream. Examples of typical lightcurves for different types of variability are shown in Figure 1. The periodic variables include pulsating stars (such as Cepheids and Miras) and eclipsing stars. Eruptive variables include T Tauri, S Doradus and pre-main sequence stars. Cataclysmic variables include novae, supernovae and symbiotic variables. The relative frequencies with which these stars occur are not important in our analysis. All that matters is that the gamut of shapes is well-represented in the training set. We are therefore interested as much in regular representatives as in extreme examples of the lightcurves. Lightcurves for the variable stars are selected from the sources listed in Table 1. For long data sequences, the experimental window is placed randomly on the lightcurve. In this way, we ensure that the bumps in the lightcurves do not occur in a privileged place.

Finally, there are lightcurves randomly chosen from the MACHO database (specifically, from field 113 towards the Bulge). The rationale for this is that instrumental artefacts are certainly present in the MACHO lightcurves and it is important for the neural network to be able to recognise these.

The training set contains 400 microlensing lightcurves, 150 stellar variable lightcurves and 200 MACHO lightcurves. The validation set contains the same number of lightcurves, although the individual representatives are obviously different. The test set are the ~ 5000 lightcurves from MACHO tile 113.18292 which is part of field 113 towards the Galactic

bulge. Let us note that – compared with real data from a variability survey – microlensing events are over-represented in our training and validation sets. The consequence of this is that the network will provide more false positives (as the prior probability of microlensing is too high). This is highly desirable, as the best approach to detecting such an intrinsically rare phenomenon as microlensing is to force fewer false negatives at the expense of more false positives.

4.2 Pre-Processing

In many applications, it is both customary and advantageous to pre-process data for feeding to the neural network. The main problem with using raw photometry data is the curse of dimensionality (see Bishop 1995, chapter 8). The simplest way of overcoming this is to extract features of the lightcurve and use this as input to the network. Properly implemented, this can lead to a very efficient network, as prior knowledge can be incorporated and redundant variables can be discarded in the pre-processing. However, there are dangers as well, as important features in the lightcurves can be erased.

The aim of a neural network is not to model the patterns but to model the decision boundary between the patterns. In microlensing surveys, event identification normally proceeds by making sequences of cuts, in which case the decision boundary is formed by a set of hyperplanes. The advantage of a neural network over conventional sequences of straight line cuts is that the former offers a better chance of describing a complicated decision boundary accurately.

Microlensing events are characterised by the presence of a (iv) single, (iii) symmetric, (ii) positive (i) excursion from the baseline. The event itself is characterised by (v) a timescale. Motivated by these five features, we extract from the lightcurves the following five parameters, which are inputs to the neural networks.

The first x_1 is the maximum value of the autocorrelation function. This helps to discriminate against noise and identify the presence of any signal. The second x_2 is calculated as follows. First, we compute the median of the flux measurements which gives a good approximation to the baseline. We then compute the mean of the datapoints lying above and below the median and finally take their ratio. This is then mapped on the interval $[0.5, 1]$ with the logistic function. The input x_2 tests for the positiveness of the excursion. The third x_3 is the maximum value of the cross-correlation function of the lightcurve with the time-reversed lightcurve. This provides a test for symmetric events. The fourth x_4 is the mean frequency $\langle \nu \rangle$ calculated with the power spectrum $P(\nu)$ as a weighting function. For a periodic variable, we expect a shift in the weighted mean frequency from zero. We compress x_4 with the logistic function to lie in the range $[0.5, 1.0]$. Finally, the fifth x_5 is the width of the autocorrelation function, as judged by its standard deviation. If the event is microlensing, then the width is a rough indication of the timescale.

To motivate this choice of inputs, Figure 2 shows the locations of all the patterns in the validation and training sets. The desideratum is that the choice of inputs offers a clear separation between microlensing events and other patterns in the five dimensional space (x_1, \dots, x_5) . The projections of this space onto the principal planes offer grounds for believ-

ing this, as there is already good partial separation in some of the plots (e.g., x_1 versus x_3) and good evidence for regularities in others (e.g., x_1 versus x_2). The final proof that the choice of inputs is good can, however, only be provided by the performance of the network on the test set.

Note that Figure 2 plots unnormalized input variables; however, the neural network uses normalized inputs. Scaling of the inputs to numbers of the order of unity is often useful, as this means that the network weights also typically take values of the same order (Bishop, 1995, chapter 8). Pictorially, this can be thought of as requiring the hyperplanes associated with each hidden unit to intersect close to the origin and near the center of the datacloud. For each input variable, this scaling is done by subtracting the mean and dividing by the standard deviation to give the normalized inputs.

So far, we have skirted round the problem of missing datapoints. For MACHO data, $\sim 10\%$ of the lightcurves have gaps of the order of a few days (aside from the 5 month gaps when the Galactic bulge is not visible from Australia). To compute the correlation functions, the data is treated as if it were uniformly sampled. This gives rise to some errors. If the typical gap size is much smaller than the event timescale, then any errors we have introduced by this procedure will be small. If the gap size relative to the timescale is very large, then no classification can be plausibly extracted. If the gap size is of the same order as the timescale, then the experiment needs re-designing. The input most sensitive to missing data is x_4 because this requires computation of the power spectrum. There are, however, existing algorithms to do this for unevenly sampled data (e.g. Lomb's periodogram as implemented by Press & Rybicki (1989) and Press et al. (1992)), which we employ.

Note that pre-processing gives rise to fast and powerful neural networks, but it can also cause loss of potentially important information in the data. To check this, we can allow a neural network itself to perform the projection. This leads to much bigger neural networks which consequently take longer to converge. However, it does have the advantage that no assumptions are built in from the beginning. In this spirit, we experimented with a big neural network which takes as the two input layers the unadulterated flux measurements and errors at the sampling times and has ~ 200 hidden neurons. Once converged, the performance of this big network is similar to the performance of smaller networks on pre-processed data. From this, we draw the conclusion that our pre-processing has not caused any serious degradation of information in the data.

4.3 Training

In training, the weights are initialised to random values. We then perform iterations to reduce the error function

$$E^n = - \sum_n (t^n \log y^n + (1 - t^n) \log(1 - y^n)) \quad (7)$$

where t^n and y^n are the target and the response of the output neuron for the n th pattern. We have chosen this form of the error function (the so-called *cross-entropy* error function) as appropriate for two class problems (see e.g., Bishop 1995, section 6.7). Given our choice of activation (3) and er-

ror functions (7), the output y^n approximates the posterior probability $P(\text{microlensing} | \text{inputs})$.

The neural network must be able to generalise from the patterns in the training set, and not merely reproduce them. A worry is that the network will be over-trained and will reproduce structures of the decision boundary in unnecessary detail. To guard against this, we use early stopping as illustrated in Figure 3. The performance of the network on the validation set is compared to that on the training set and the training stopped just before the error in the validation set rises. Another safeguard is provided by the introduction of a small amount of noise to the weights on each iteration, which guards against entrapment in a local minimum.

If training is started from different initial weights, we converge to slightly different final weights. This makes it advantageous to use a committee of 10 neural networks (Bishop 1995, section 9.6). There are a total of 1500 lightcurves available. For each member of the committee, the 1500 patterns are split in half randomly to give validation and training sets with 750 members. For each pattern, the final output is the average of the output of all 10 neural networks.

The histogram of the output values for the combined validation and training set is shown in Figure 4. There is a very clean separation of microlensing events and other forms of variability. The non-microlensing events are strongly peaked at a probability $y = 0$, but there are a few events (~ 10) that extend up to $y = 0.2$. The microlensing events are strongly peaked at $y = 1$, although again there are a few (~ 10) that extend down to $y = 0.7$. The probability $y = 0.5$ corresponds to the formal decision boundary (Bishop 1995, section 10.3). In fact, between $0.2 < y < 0.7$, there are almost no events in the histogram. If, when presented with a lightcurve, the neural network does give an output in this range, then the classification is in reality uncertain. This is because any error in the output can cause it to straddle the formal decision boundary. This range of outputs really corresponds to patterns that are not present in the training and validation sets. This is valuable as it offers the possibility of the detection of unexpected and novel events in variability surveys.

There are just 3 microlensing events out of 800 that are misclassified (i.e., have $y < 0.5$). These are scarcely visible on the histogram. It is interesting to locate these events in our input space (see Figure 2). These events have input coordinates $(-1.44, -1.07, -1.20, -1.17, -1.00)$, $(-1.40, -1.16, -1.16, -1.14, -0.8)$ and $(-1.32, -1.11, -1.0, -1.11, -0.8)$. They are small amplitude or short duration events dominated by noise, as indicated by the value of the x_1 input which measures the presence of the signal. There is 1 false positive (i.e., a non-microlensing lightcurve with $y > 0.5$), which has coordinates $(-1.5, -0.7, -1.23, -1.2, -1.1)$. This is a lightcurve from the MACHO tile which is probably neither microlensing nor variable star, but just noise.

5 TESTS TOWARDS THE BULGE FIELDS

5.1 Normal Events

All MACHO lightcurves extracted with conventional PSF photometry (such as SoDoPhot) are now publically available (Allsman & Axelrod 2001). As a first test, we use lightcurves

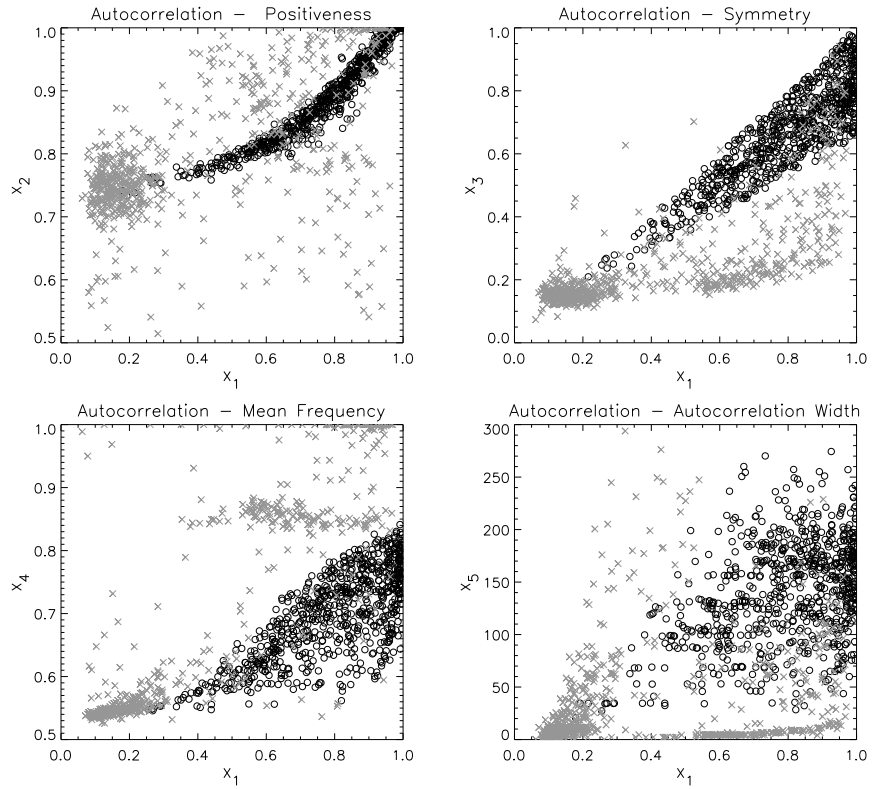


Figure 2. This shows projections onto the principal planes of the five-dimensional space of inputs. Bold circles show the microlensing events and grey crosses the variable stars and noise in the training and validation sets.

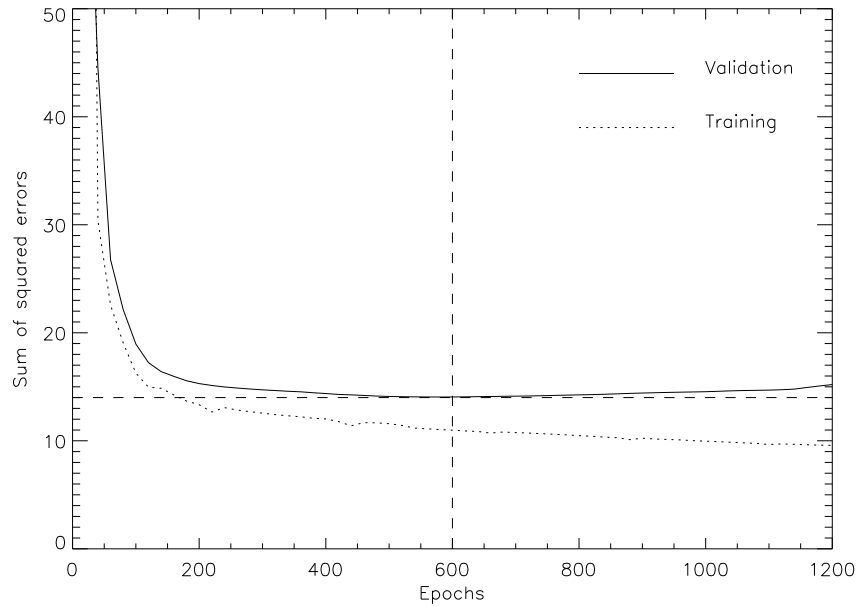


Figure 3. This shows the value of the cross-entropy error function versus the epochs of training (number of iterations) for the patterns in the training and validations sets. The long-dashed line shows the point at which the training is stopped. The sum of errors is ~ 15 out of the 700 patterns in the set.

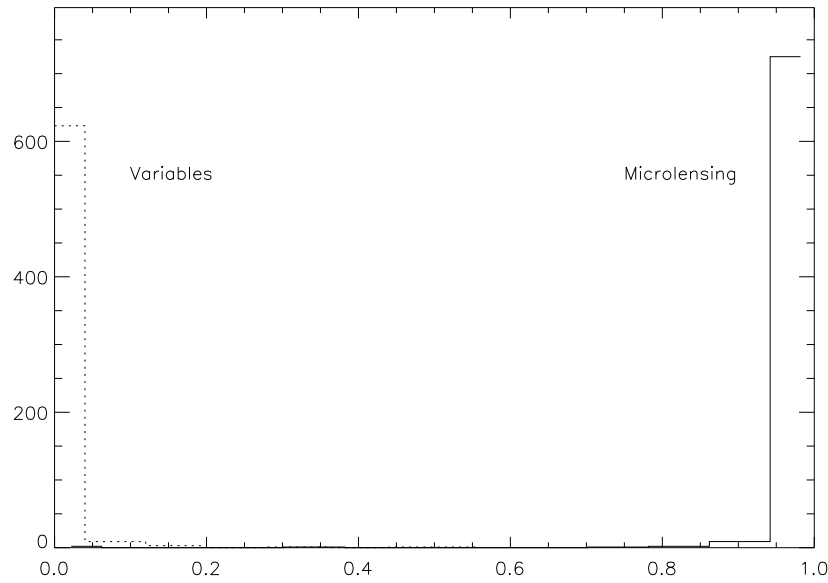


Figure 4. This shows the histogram of output values for the 1500 patterns in the validation and training sets. Note the clean separation between microlensing and other types of variability.

ID	MACHO ID	R	B	ID	MACHO ID	R	B
1	97-BLG-24	0.93	1.00	2	95-BLG-5	0.92	0.96
3	97-BLG-42	0.00	0.00	4	97-BLG-s4	0.72	0.00
5	95-BLG-15	0.00	0.00	6	95-BLG-s8	1.00	1.00
7	97-BLG-18	1.00	1.00	8	96-BLG-26	1.00	1.00
9	97-BLG-38	0.64	0.47	10	97-BLG-58	1.00	1.00
11	96-BLG-1	1.00	1.00	12	97-BLG-2	1.00	1.00
13	96-BLG-14	0.00	0.00	14	95-BLG-s9	0.99	0.91
15	96-BLG-21	0.68	0.00	16	95-BLG-1	1.00	1.00
17	96-BLG-s10	-	0.16	18	96-BLG-20	0.99	1.00
19	96-BLG-10	0.99	0.90	20	95-BLG-4	0.81	0.02
21	95-BLG-23	0.00	0.00	22	95-BLG-s13	0.64	0.05
23	95-BLG-10	1.00	1.00	24	97-BLG-4	0.00	0.00
25	97-BLG-16	1.00	0.23	26	96-BLG-8	0.96	0.99
27	95-OGLE-16	0.99	-	28	95-BLG-39	0.16	1.00
29	95-BLG-3	0.39	0.00	30	97-BLG-37	1.00	1.00
31	97-BLG-14	0.21	0.00	32	95-BLG-11	0.01	0.00
33	96-BLG-31	0.81	1.00	34	96-BLG-s16	1.00	0.83
35	97-BLG-s14	0.80	0.90	36	95-BLG-22	0.30	0.79

Table 2. This shows the output of the committee of neural networks on the subset of candidates towards the bulge in Alcock et al. (2000b) which are selected on the basis of the conventional PSF photometry package (SoDoPhot). The results of the analysis of the red and blue lightcurves are shown separately. The output is the probability that the event is microlensing. (Note that the red data for event 17 and the blue data for event 27 are unavailable).

from tile 18292 of field number 113, which lies towards the Galactic bulge. This tile contains ~ 5000 lightcurves of which one was identified by MACHO as a microlensing event. The MACHO data are taken at a site with moderate seeing. According to Alcock et al. (2000b), the median seeing is ≈ 2.1 arcsec. This means that the quality of the data is sometimes quite poor. To allow for this, we clean the lightcurves by removing all isolated points with more

than 3σ deviation from the immediately preceding and succeeding datapoints. In general, this makes good sense as it removes outliers, but it can sometimes remove meaningful datapoints for very rapid brightness variations.

Each cleaned lightcurve is shown to the committee of neural networks. The red and blue passband data are analysed separately. In principle, it would be advantageous to analyze the red and blue data together because most variable

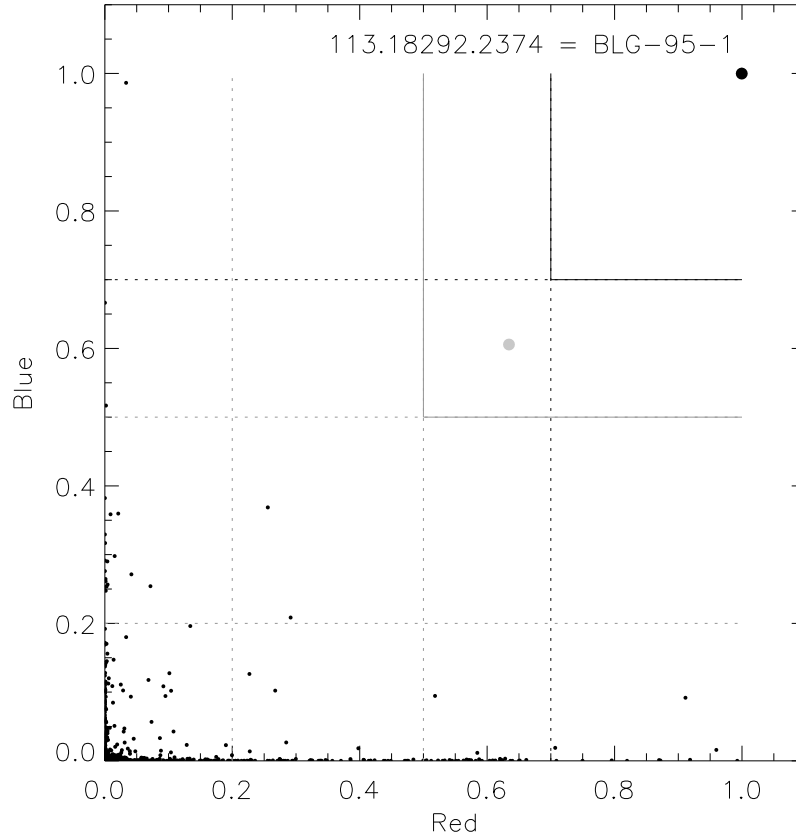


Figure 5. This shows the output of the committee of neural networks for all lightcurves in tile 113.18292, which is publicly available from the MACHO project website (see Allsman & Axelrod 2001). Shown on the vertical and horizontal axes are the probabilities that the blue and red lightcurves are microlensing. There are ~ 5000 lightcurves on the tile, including one event BLG-95-1 identified by the MACHO collaboration as microlensing. This is shown as the black spot.

stars show chromaticity differences. However, this option is not open to us at the moment because the publicly available colour information on variable stars is still quite limited. Figure 5 shows the results of the deliberations of the committee. The probability of microlensing given the blue data is shown against the probability given the red data. There is only one pattern that satisfies this, namely the event identified by MACHO as BLG-95-1. It is clearly and cleanly separated from the rest of the patterns in the figure as a black circle in the topmost right corner. There is an additional pattern that has output values $y \approx 0.6$ for both the red and blue data. This falls within the regime of novelty detection. Its input coordinates are $(-0.6, -1.5, -0.8, -0.66, 1.26)$. It is a very long event since $x_5 = 1.26$ is higher than typical values for microlensings. It falls into poorly-sampled region in Figure 2 which suggests why this low signal-to-noise lightcurve was dragged into the microlensing range. Its lightcurve is shown in the upper panel of Figure 6. It is most probably a form of stellar variability that does not lie in the training and validation sets. It is interesting to note that there are a number of lightcurves with output greater than 0.9 in one band, but not in the other. Shown in the lower panel of Figure 6 is a typical example, in this case securely iden-

tified in blue ($y > 0.95$) but not in red ($y < 0.05$). The blue lightcurve does indeed look like a microlensing event, but the better sampling in the red passband shows a highly active many-humped lightcurve which is most probably an eruptive variable.

As a second test, we analyze the lightcurves for all 36 events in Alcock et al (2000b) that were identified on the basis of conventional PSF photometry. Table 2 shows the results of the poll of the committee. In each case, the output of the neural network on the red and the blue data is given. Of course, it is important to bear in mind that the MACHO group's classification algorithm is itself probably not 100 per cent efficient. There are reasons to believe – both from the very high rate towards the Galactic Center that is incompatible with theoretical models of the Galaxy and from the differences between the MACHO and EROS results – that the subsample of candidates found by MACHO may have some contamination. There are total of 19 events identified with a probability $\gtrsim 0.5$ as microlensing in both the red and blue filters. In fact, these events are all beyond reproach as microlensing candidates as the probability $\gtrsim 0.9$. Events 28 and 36 are securely identified in the blue data, but the red data is corrupted. Events 4, 9, 15,

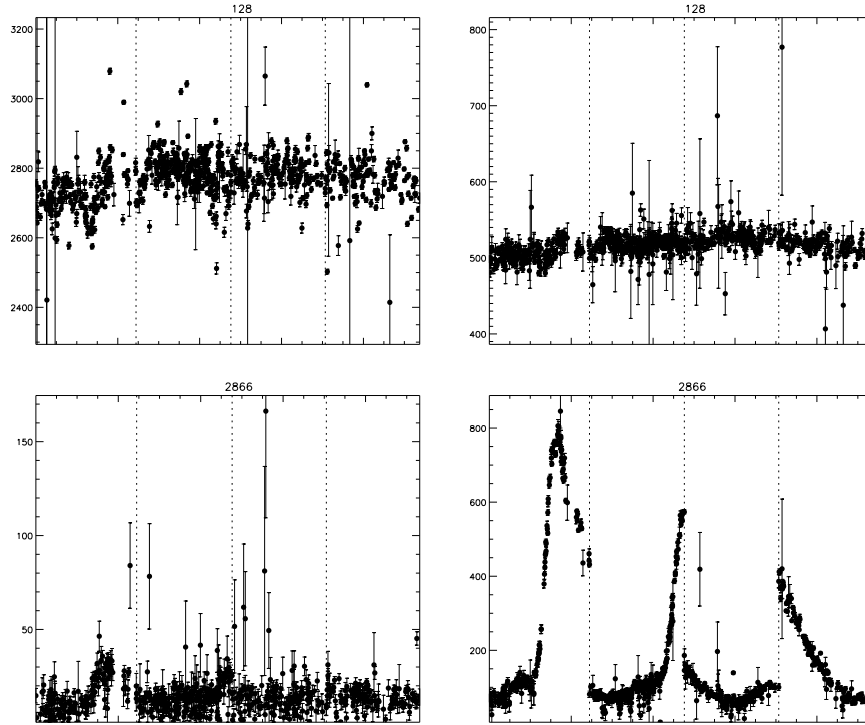


Figure 6. The upper panels show the blue and red lightcurves for the event identified by the grey spot in Figure 5. The lower panels show the lightcurves for the event securely identified in blue (left panel), but not in red (right panel). In all cases, the horizontal axis is time in days, the vertical axis is flux in ADU/s.

20, 22 and 25 are identified in the red data, but not in the blue. Lastly, there are 9 events for which no microlensing signal whatsoever is detected (event numbers 3, 5, 13, 17, 21, 24, 29, 31, 32). We shall examine the lightcurves of some of these events shortly, but for the moment let us emphasise that there is no guarantee that the original identification by the MACHO collaboration was correct.

Fig 7 shows the contours of probability for the training and validation sets in the input space. Light gray means that the probability is greater than 0.5 and corresponds to the formal decision boundary (see Bishop 1995, section 10.3). Dark gray means that the probability is greater than 0.9 and corresponds to almost certain microlensing. The irregularity of the contours is due to the fact that some regions are poorly sampled in the training and validation sets. The contours have been drawn with a view to guiding the eye. Superposed on the contours in Fig 7 are the events. The nine unfilled circles are those identified by the network as variable stars but by MACHO as microlensing events. The black circles are those for which both MACHO and the network agree as microlensing.

There are a number of things to notice in the diagram. First, it is evident that the network has the ability to extrapolate from the validation and training sets and assign relative importance to the combinations of features extracted by the input variables. This is clear because there are events securely identified although they lie outside the contours (for example, event 18 is unambiguously identified despite ly-

ing outside the probability contours in the two top panels). Second, the x_4 input is the only one for which explicit allowance has been made for noise and sampling. The network seems to assign greater importance to this input, as almost all the filled circles lie within the projected 90% probability contour. This suggests that further improvements may be possible by allowing for noise in the extraction of other input parameters (for example, using extirpolation for the correlation analysis). Third, the separation between the 0.5 and 0.9 probability contours is typically very small, so the contour surface is very steeply rising. Such outputs can correspond to novelty detection. Accordingly, they occupy only a small region of the input space and so novelty detection occurs – as is highly desirable – for only a few lightcurves. The small separation between the contours provides justification for the sizes of the training and validation sets. If there are too few patterns in these sets, then the separation would widen. Such widening happens in our network only in a few unimportant regions, which are physically inaccessible (that is, such a combination of input variables gives rise to lightcurves that do not occur in nature). Fourthly, all the unfilled circles have $x_1 < -0.8$ and so lie in the noise-dominated regime. However, the values of x_2 indicate the presence of substantial positive excursions. This is already enough to tell us that the noise in the MACHO data is strongly non-Gaussian.

Figure 8 shows the lightcurves for 8 of the events corresponding to the unfilled circles. For some of these events,

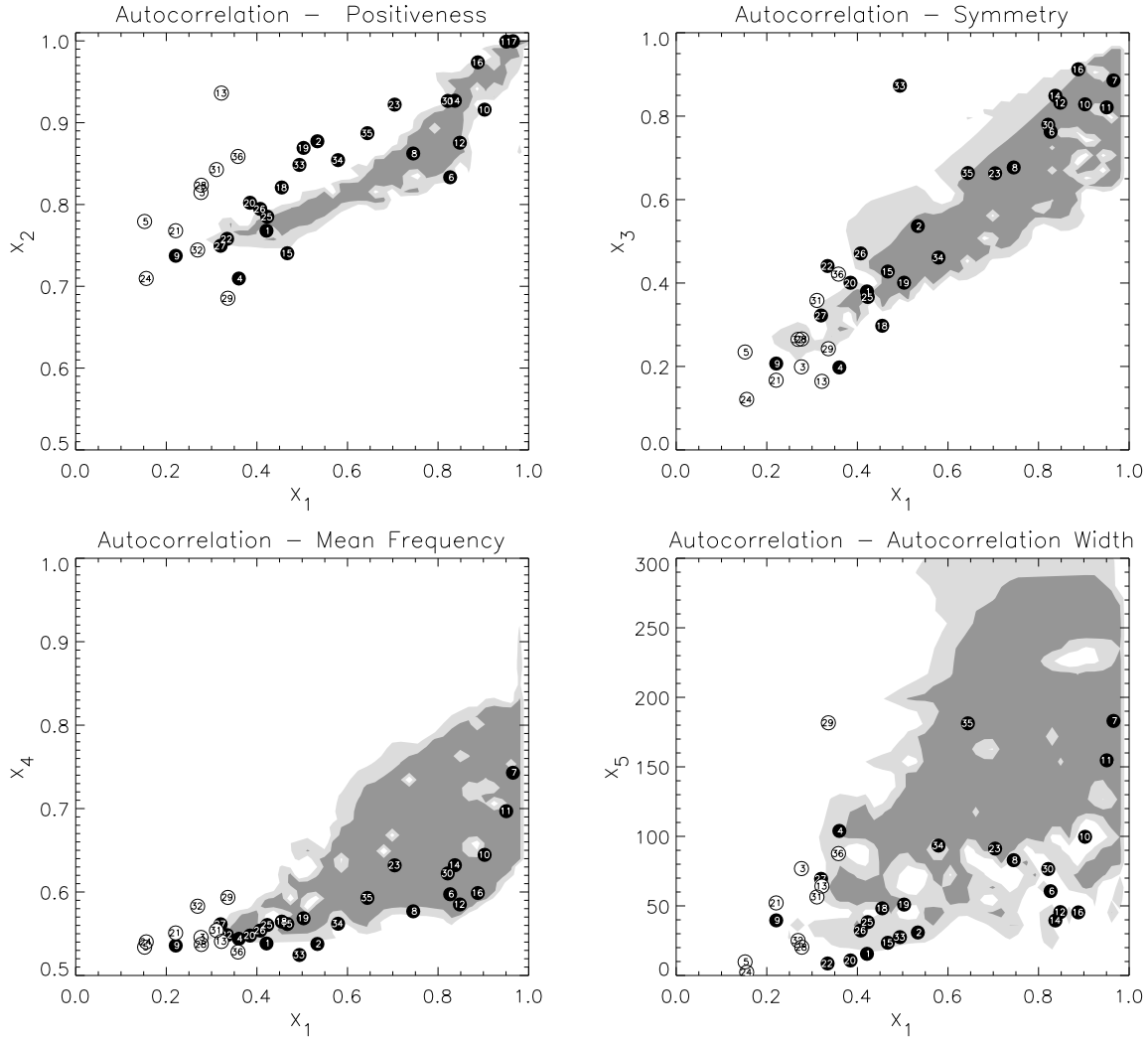


Figure 7. The grey-scale contours show the probability of microlensing in the input space (x_1, \dots, x_5) as judged from the patterns in the training and validation sets. The circles show the locations of the microlensing events identified by MACHO using conventional PSF photometry. Filled circles designate the events also identified in the red filter by the network. Unfilled circles are not identified. Numbers within circles refer to our event designations in Table 2. (Light grey means that the probability is greater than 0.5, dark grey greater than 0.9).

it looks as though there are secondary bumps (e.g., event 3). For others, the bump is not properly contained (e.g., events 5 and 31) or the bump is overwhelmed by noisy data (e.g., events 13 and 17). It seems that the performance of our network is excellent, as these events certainly need to be looked at with care before accepting a classification as microlensing. However, it is premature to conclude that MACHO have misclassified these events. This is because the MACHO group have re-processed all the lightcurves with difference image analysis (DIA) and this will improve the quality of the lightcurves, reducing noise and contamination from nearby stars. However, without having the DIA lightcurves, we cannot confirm their verdict of microlensing.

ID	MACHO ID	deviation	R	B
1	95-BLG-30	f	1.00	1.00
2	96-BLG-12	p	1.00	0.99
3	97-BLG-1	b	0.95	1.00
4	97-BLG-8	p	1.00	1.00
5	97-BLG-26	p	1.00	1.00
6	96-BLG-3	b	0.83	0.51
7	95-BLG-18	p	0.99	0.75

Table 3. This shows the output of the committee of neural networks on the exotic events identified towards the bulge in Alcock et al. (2000b). These are all exotic events selected on the basis of the conventional PSF photometry package (SoDoPhot); f stands for deviations due to finite source size, p due to parallactic effects and b due to binarity. The output is the probability that the red and blue data correspond to a microlensing event.

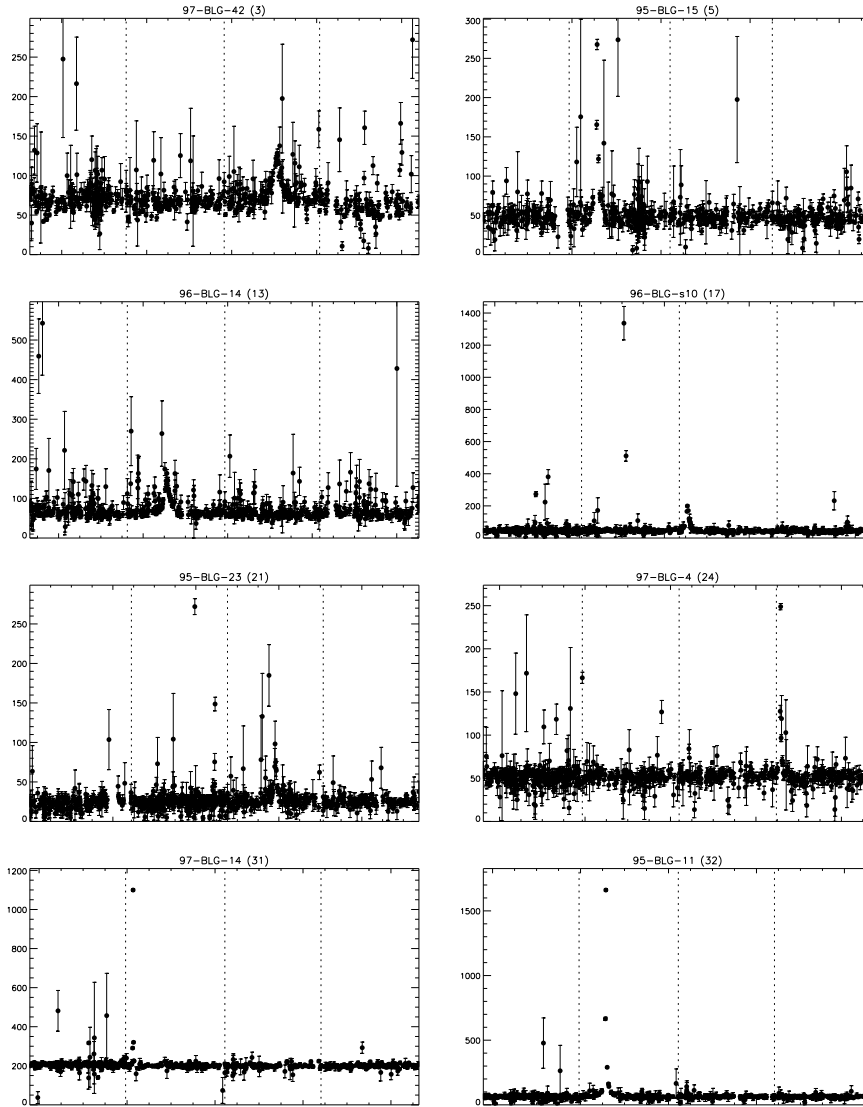


Figure 8. This shows the datapoints for eight of the events classified as non-microlensing by the network and as microlensing by the MACHO collaboration. The vertical axis is flux in ADU/s and the horizontal axis is time in days. The data is presented as four strips of 7 month sequences; the 5 months when the bulge is not visible from Australia is marked by the vertical dashed lines.

5.2 Exotic Events

Some microlensing lightcurves can show deviations from the standard Paczyński form caused by parallax or finite-source size effects or by binarity and so on (see e.g., Mao & Paczyński 1993, Mao & Di Stefano 1995, Kerins & Evans 1999, Mao et al. 2002). In Table 3, all the exotic events identified in Alcock et al. (2000b) using the SoDoPhot photometry package are processed with the committee of neural networks.

Parallax events (like 96-BLG-12) occur when the Einstein radius projected onto the observer’s plane is of the order of an astronomical unit. In such a circumstance, the changing motion of the Earth around the Sun during the event is detectable by an asymmetry in the lightcurve with respect to the peak. Events showing deviations caused by finite source size (like 95-BLG-30) occur whenever the an-

gular size of the source is of the same order of magnitude as the angular Einstein radius. They are usually flatter-topped than the classical Paczyński curves for microlensing by a point source. For both these kinds of deviation, the committee of neural network performs well, as shown in Table 3. All the parallax and finite source size events are identified as microlensing.

However, binarity can cause much substantial deviations. For example, strong binary events have additional peaks, although these can sometimes be missed if sampled irregularly. Weak binary events may just have distortions to the peak or the wings of the lightcurve. Accordingly, we might expect the detection of binary lightcurves to require the training and testing of a new neural network. This is supported by the results in Table 3. Here, 96-BLG-12 is identified by the committee, whereas 96-BLG-3 falls into

the domain of novelty detection. It is reassuring that in the former case, the event is recognised, while in the latter case, the event is recognised as a new phenomenon. The development of software to recognise binary events is a problem that has not been fully solved by any of the microlensing collaborations to date. It seems reasonable to expect neural networks to play a powerful role here.

6 CONCLUSIONS

This paper has devised a working neural network that can distinguish simple microlensing lightcurves from other forms of variability, such as eruptive, pulsating, cataclysmic and eclipsing variables. The network is structured to have five input neurons and one output neuron. The inputs and output are separated by a layer of hidden neurons. The simplicity of the network means that it can be trained very quickly and it can be used to process huge datasets in less than a second. Each lightcurve is pre-processed to provide five inputs to be fed to the network. In our application, the five inputs were chosen on physical grounds as good discriminants for microlensing. In other applications, different input variables may be optimum. Our network has been constructed so that the output is the posterior probability of microlensing.

We believe that neural networks offer three important advantages over conventional techniques using in microlensing experiments. First, the decision boundary separating microlensing from non-microlensing may be rather complicated. At present, all microlensing collaborations use a series of cuts (for example, on the goodness of fit to a Paczyński curve, on achromaticity and so on). This is the crudest form of the decision boundary. However, even simple neural networks can reproduce complicated decision boundaries and so the technique is both more efficient and more flexible. Moreover, once a lightcurve has failed to pass a cut at the early stages of a conventional selection process, it is lost for any further analysis. But, neural networks assign relative importance to the input parameters, thus the decision is based on the whole of the information available.

Second, neural networks offer a superior way of calculating the event rate avoiding the need for any kind of efficiency calculation. The classical procedure of identifying events with cuts is inefficient, and this necessitates the cumbersome Monte Carlo calculation of the numbers of synthetic events passing the cuts. However, a properly-designed neural network can reproduce the decision boundary well and can enable the event rate to be computed directly for comparison with theoretical models, thus completely sidestepping the need for any Monte Carlo calculation of the efficiencies.

Third, novelty detection is made both more precise and easier by neural networks. The conventional approach relies on examination by eye of the events left over after applying a sequence of cuts. For our neural network, we have argued that all lightcurves with outputs between 0.2 and 0.7 may be examples of lightcurves not contained within the training set. These are the events which need looking at very carefully. In the even more massive datasets of the future, it will be important to identify possible novel events as quickly and as efficiently as possible.

From the point of view of microlensing, it is interesting to extend the work in this paper to include additional

effects. Some of the ongoing microlensing experiments are working in the highly blended régime. For example, the POINT-AGAPE (Paulin-Henriksson et al. 2002a,b), WeCAPP (Riffeser et al. 2001) and MEGA (Crotts et al. 2000) collaborations are all monitoring the nearby galaxy M31. Here, the individual stars are not resolved, so the flux in a pixel or superpixel is followed (Baillon et al. 1993). The range of lightcurves in such pixel lensing experiments is very wide – for example, microlensing events can occur in the same superpixel as bright variable stars (e.g., the event PA-99-N1 described in Aurière et al 2001). So, the identification of microlensing events becomes still more daunting. As the complexity of the pattern recognition task increases, so we expect the power and flexibility of the neural network approach to pay increasing dividends. Also, in this paper, we have concentrated on the microlensing datasets towards the bulge, for which the source stars are often bright. It is important to apply our techniques to the microlensing events towards the Large Magellanic Cloud. Here, the task is harder as the source stars are fainter and there is serious contamination from supernovae in background galaxies. This work will be the subject of a separate publication.

Although our application has been strongly focused on microlensing, the technique is of general applicability in astronomy. There are numerous ongoing or planned massive photometry surveys using robotic telescopes (ROTSE), wide field cameras (WASP and VISTA) and space-borne satellites (GAIA and Eddington). Although the goal of the surveys is different, the basic method is the same – brute force search through many terabytes of data for interesting but rare events, whether planetary transits, cataclysmic variables or optical flashes. We envisage such tasks being routinely devolved to neural networks in the astronomy of the future. In each case, cascades of neural networks could be trained to filter and identify the various classes of variable stars, to pinpoint the target events of interest and to isolate the unexpected or new classes of phenomenon which need looking at very carefully.

7 SPECULATIONS

Suppose the goal is to monitor the whole sky for variability at short time intervals down to 20th magnitude (roughly a billion objects in our Galaxy). In this speculative final section, we ask what is possible now and what will be possible by 2010?

Let us consider the simple situation of a single neural network program running on a single computer. The middle-range hardware situation today is typically a processor running at 2200 Mhz (corresponding to approximately 1000 MIPS or Million Instructions per Second). In order to predict the situation in 2010, we can use “Moore’s Law”, which says that the numbers of transistors in a processor chip doubles every year or so. Thus, by 2010 the processor speed should be $\sim 100\,000$ MIPS, compared to about 1000 MIPS today. But, to evaluate the progress in run time, we must consider both hardware and the compiler. Benchmarking programs such as SPEC provide us with some clues as to what will be achieved in 2010. If we look at the evolution in performance results on SPEC tests for computers between 1995 and 2000, we find an approximate speed-up

factor of 16, or roughly 1.74 per year. We can extrapolate this progress over the 2002-2010 period, which gives a speed-up factor of 85. In other words, both Moore's Law and the extrapolation of benchmarking suggest rather similar speed-up factors of roughly two orders of magnitude by 2010.

The time required to run the neural network itself is negligible compared to the time required to run the pre-processing, which extracts the parameters used by the neural network. Our present pre-processing program requires 10^{-4} s to analyse 100 data points for a single star. We have chosen 100 datapoints as it might correspond to sampling 3 times a night for one month, which is reasonable for the detection of fast transient events. Alternatively, it might correspond to sampling once a night for 3 months, which is reasonable for the detection of variability like microlensing with a characteristic timescale of ~ 1 month. At present, it therefore takes $\sim 10^5$ s (or over a day) to analyse such dataset for the whole sky. By 2010, it will take only 20 minutes for such a program to run on the whole sky (using the speed-up factor of 85). More generally, the time taken in seconds to analyse a set of N_{pts} data points for N_* stars in 2010 is

$$t \sim 2 \times 10^{-9} N_* N_{\text{pts}} \log N_{\text{pts}}. \quad (8)$$

Let us assume there are 8 hours of observing time a night and that we wish to process a months data for the whole sky in real-time. Then we can derive the real-time equation

$$t^2 \sim 1.7 \times 10^6 (13.7 - \log t). \quad (9)$$

which has a solution $t \sim 50$ minutes. In other words, real-time processing of variable phenomena across the entire sky down to 20th magnitude will be possible for sampling rates of $\gtrsim 1$ hr by 2010.

Our speculative calculation errs on the pessimistic side because we have not taken into account any correction for application of parallel processing or the fast developing GRID technology for high performance computing. However, it surely does enough to convince the reader that, properly trained, neural networks can analyse huge datasets very quickly. This will become one of the methods of choice for data-mining in the massive variability surveys of the very near future.

ACKNOWLEDGMENTS

VB is supported by a Dulverton Scholarship. YLD thanks PPARC, while NWE thanks the Royal Society for financial support. In this research, we have used, and acknowledge with thanks, data from AAVSO International Database based on observations submitted to the AAVSO by variable star observers worldwide. This paper also utilizes public domain data obtained by the MACHO Project, jointly funded by the US Department of Energy through the University of California, Lawrence Livermore National Laboratory under contract No. W-7405-Eng-48, by the National Science Foundation through the Center for Particle Astrophysics of the University of California under cooperative agreement AST-8809616, and by the Mount Stromlo and Siding Spring Observatory, part of the Australian National University. In this respect, we particularly wish to thank Robyn Allsman and Tim Axelrod for help in acquiring data for an entire tile. We also thank the anonymous referee for a helpful report.

REFERENCES

- Alcock C. et al. 1997, ApJ, 486, 697
- Alcock C. et al. 2000a, ApJ, 542, 281
- Alcock C. et al. 2000b, ApJ, 541, 734
- Allsman R.A., Axelrod T.S. 2001, astro-ph/0108444
- Andreoni S., Gargiulo G., Longo G., Tagliaferri R., Capuano N. 2000, MNRAS, 319, 700
- Ansari R. et al. 1995, AA, 299, L21
- Ansari R. et al. 1996, AA, 314, 94
- Antonello E., Morelli P.L. 1996, AA, 314, 541
- Aurière M. et al. 2001, ApJ, 553, L137
- Bailer-Jones C.A.L., Irwin M., Gilmore G., von Hippel T. 1997, MNRAS, 292, 157
- Baillon P., Bouquet A., Giraud-Heraud, Y., Kaplan J. 1993, AA, 277, 1
- Bishop C., 1995, Neural Networks for Pattern Recognition, Oxford University Press, Oxford
- Bracewitz H.K., Dworak T.Z. 1980, Acta Astron, 30, 501
- Conway A.J. 1998, New Astronomy Reviews, 42, 343
- Crotts A., Uglesich R., Gould A., Gyuk G., Sackett P., Kuijken K., Sutherland W., Widrow L. 2000, In "Microlensing 2000: A New Era of Microlensing Astrophysics", eds. J.W. Menzies and P.D. Sackett, ASP Conference Series, vol. 239, p. 318, ASP, San Francisco.
- Hamuy M., Phillips M.M., Suntzeff N.B., Schommer R.A., Maza J., Smith R.C., Lira P., Aviles R. 1996, AJ, 112, 2438
- Kerins E.J., Evans N.W. 1999, ApJ, 517, 734
- Lahav O. et al. 1995, Science, 267, 859
- Lasserre, T. et al. 2000, AA, 355, L39
- Mao S., di Stefano R. 1995, ApJ, 440, 22
- Mao S., Paczyński B. 1991, ApJ, 374, L37
- Mao S. et al. 2002, MNRAS, 329, 349
- Müller B., Reinhardt J., Strickland M.T. 1995, Neural Networks: An Introduction, Springer Verlag, Berlin
- Paczynski B. 1986, ApJ, 304, 1
- Paczynski B. 2001, In "Mining the Sky", eds A.J. Banday, S. Zaroubi, and M. Bartelmann, p. 481, Springer Verlag, Berlin (astro-ph/0110388)
- Paczynski B. 2002, In "Small Telescope Astronomy on a Global Scale", eds W.P. Chen, C. Lemme, B. Paczyński, ASP Conference Series, vol 246, in press, ASP, San Francisco. (astro-ph/0108112)
- Paulin-Henriksson S. et al. 2002a, ApJ, 576, L121
- Paulin-Henriksson S. et al. 2002b, astro-ph/0207025
- Perdang J., Serre T. 1998, A&A, 334, 976
- Press W.H., Rybicki G.B. 1989, ApJ, 338, 277
- Press W.H., Teukolsky S., Vetterling W.T., Flannery B. 1992. Numerical Recipes, Cambridge University Press, Cambridge, 2nd ed. chap. 13.
- Riffeser A. et al. 2001, AA, 379, 362
- Storrie-Lombardi M.C., Lahav O. 1994, Vistas in Astronomy, 38, 249
- van Genderen A.M. 1995, AA, 304, 415
- Udalski, A., Szymanski, M., Kaluzny, J., Kubiak, M., Mateo, M., Krzemiński, W., & Paczynski, B. 1994, Acta Astronomica, 44, 227
- Wozniak P.R. et al. 2001, American Astronomical Society Meeting, 199, 130.04